Available online at www.sciencedirect.com
ScienceDirect
Experimental Thermal and Fluid Science 31 (2007) 333–347
Experimental Thermal and Fluid Science
www.elsevier.com/locate/etfs

Experimental investigation of fluid dynamic instability in a transonic cavity flow

Hiroyuki Hirahara [a,*], Masaaki Kawahashi [a], Maksud Uddin Khan [b], Kerry Hourigan [c]

[a] Department of Mechanical Engineering, Faculty of Engineering, Saitama University, 255 Shimo-Okubo, Sakura, Saitama 338-8570, Japan
[b] Toyama University, 3190 Gofuku, Toyama, Toyama 930-8555, Japan
[c] Fluids Laboratory for Aeronautical and Industrial Research (FLAIR), Department of Mechanical Engineering, Monash University, VIC 3800, Australia

Received 19 August 2005; accepted 15 May 2006

Abstract

The acoustic and fluid dynamic resonance in a two-dimensional cavity flow was investigated experimentally. In order to visualize a periodic oscillation of the shear layer and the behavior of vortices, the schlieren method was used with an ordinary CCD camera and a high-speed video camera. Particle image velocimetry (PIV) measurements were also carried out to obtain the vorticity distribution during the oscillation in the cavity flow. Shedding and interaction of vortices in the shear layer were observed near the trailing edge of the cavity, which causes the generation of pressure waves. The feedback process of the oscillation was determined using high-speed camera images. From these results, the $x - t$ diagram for the oscillation cycle was obtained. Based on the flow visualization, for Rossiter's constants, it was confirmed that the dominant acoustic mode was $m = 2$ and that $K_c = 0.5$ in the present experiment. Also, the pressure level for mode $m = 2$ was the most intense for a wide range of flow Mach numbers. The results obtained by PIV measurement show that there is outgoing and incoming flow near the trailing edge of the cavity. It was found that a very strong change of vorticity associated with the detachment and attachment of boundary layer was induced on the trailing edge due to the fluid dynamical instability.

1. Introduction

Sound oscillation in cavity flow is a well-known and fundamental problem in fluid dynamical instability. Since the original work by Helmholtz, a number of papers in this area have been published for external and internal flows. For example, Owen [1] investigated the unsteady pressure in bomb bays in a low-speed wind tunnel. He showed that for shallow and moderately deep bomb bays ($L/D > 5$), the unsteady pressure field was random essentially for air speed up to 300 ft/s. A similar investigation was carried out by Norton [2], but the speed was higher than that in the previous experiment. In addition to the random pressure fluctuations, it was found that strong periodic pressure fluctuations occurred in the bomb bay. Krishnamurty [3] investigated the periodic pressure fluctuations. He found that the fluid in a cavity oscillated over a broad range of flows in the subsonic and supersonic flow regimes. He also found that strong acoustic radiation accompanied the periodic pressure fluctuation. Plumblee [4] calculated the acoustic resonant response. The periodic pressure fluctuations were proposed to be due to an acoustic resonance excited by the unsteadiness in the turbulent boundary layer approaching the cavity. However, later this hypothesis was found to be unjustified because Krishnamurty found strong periodic pressure fluctuations when the oncoming boundary layer was laminar. Rossiter [5] put forward the most important model for the cavity oscillation. He proposed a feedback mechanism by which he was able to explain the generation of the acoustic radiation. In his paper, he proposed a fundamental physical model of the interaction

* Corresponding author. Fax: +81 48 858 3711.
E-mail address: Hirahara@lamb.mech.saitama-u.ac.jp (H. Hirahara).

0894-1777/$ - see front matter © 2006 Elsevier Inc. All rights reserved.
doi:10.1016/j.expthermflusci.2006.05.007

Nomenclature

D	depth of cavity	p_{ref}	reference pressure = 20 μPa
f	resonant frequency	$\bar{p}_f$	spectrum density of pressure amplitude
K_c	ratio of convection speed of vortices to free stream velocity	St	Strouhal number
		T	temperature
L	length of cavity	U_e	free stream velocity
M	free stream flow Mach number	u	streamwise flow velocity
m	$m_v + m_\lambda$	W	width of channel
m_v	number of vortices	α	empirical phase number between vortices and pressure waves
m_λ	number of waves		
P	sound pressure level	κ	specific heat ratio
p	pressure		

between the vortices in shear layer and propagating sounds. Following Rossiter's inference, the Strouhal number is expressed by the following equation:

$$St = \frac{fL}{U_e} = \frac{m - \alpha}{M + 1/K_c}, \quad m = 1, 2, 3, \ldots \tag{1}$$

where α is an empirical phase number between vortices and pressure waves, U_e the free stream flow velocity, K_c the ratio of the convection speed of the vortices in the shear layer to the free stream velocity, L the length of the cavity. Also, $m = m_v + m_\lambda$ is an important integer, where m_v and m_λ are the number of vortices and wave number along the resonant path, respectively. To use the above equation, we need to determine two parameters, α and K_c. Following previous studies [6], it is shown, in good agreement with experimental results, that $\alpha = 0.25$ and $K_c = 0.57$ for $0.4 < M < 1.2$.

Heller [6] improved Rossiter's empirical equation by assuming that the sound speed in the cavity is equal to the free-stream stagnation sound speed

$$St = \frac{fL}{U_e} = \frac{m - \alpha}{M/\sqrt{1 + 1/2(\kappa - 1)M^2} + 1/K_c}, \quad m = 1, 2, 3, \ldots \tag{2}$$

Later, Heller et al. [7] proposed another type of flow mechanism that drives the pressure oscillation in a cavity. In that paper, they also showed that the sound pressure level reaches its peak in the transonic flow region. Rockwell [8], in his review paper, and Rockwell and Naudascher [9] classified the cavity into three major categories, which were: a fluid-dynamic cavity which was characterized by an oscillation caused by the inherent instability of the flow; a fluid-resonance cavity, where the oscillation took place due to the resonant effects in the cavity; and lastly, a fluid-elastic cavity in which the oscillation was coupled with the motion of a solid boundary. Tam [10] and Tam and Block [11] analyzed the acoustic mode in the cavity with an acoustic theory; they applied their method to the low-speed cavity flow and showed a comparison with experimental data. Using linear theory, the fluctuation of the vortex sheet due to the pressure fields was solved.

Zhang and Edwards [12] identified two oscillatory mechanisms in a supersonic cavity flow. One was characterized by the longitudinal oscillation of the strong trailing vortex and the vortices shed downstream from the leading edge. The latter one was characterized by the transverse oscillation of a single vortex in the cavity. Sakamoto et al. [13] found that the longer cavity had a larger circulating flow and a pair of small three-dimensional vortices appeared due to the flow separation on the side walls. The structure of the flow is highly three-dimensional. The shorter cavity has only one vortex and the flow is essentially two-dimensional. Tracy et al. [14] investigated the transonic cavity flow from the L/D ratio from 4 to 20. They observed that the mode amplitude and the bandwidth depended on the Mach number. Tones were observed at the L/D ratio of 4.40 and 6.70 but not at 20. Zhang and Edwards [12] performed a numerical investigation of the supersonic cavity flow at Mach 1.5 and 2.5 with an L/D ratio of 3. They found that the oscillatory mode is a longitudinal one and the trailing edge of the cavity provides the feedback of the disturbances so that the oscillation can be sustained. Takakura et al. [15] investigated the unsteady supersonic internal cavity flows. They used the Chakravarthy–Osher TVD scheme to solve the 2D Navier–Stokes equation for the overview of the flow pattern. They also used a very large eddy simulation to capture the unsteady flow field in detail. They recognized one, two and three vortices for the cavity of $L/D = 1, 2, 3$, respectively. The research finally concluded that the important governing factor of the dominant oscillation is the motion of the mean flow rather than the shear layer itself. Takakura et al. [16] carried out computations for unsteady supersonic cavity flows using a large eddy simulation. They performed 2D and 3D computations for the unsteady supersonic cavity flow, and were able to capture the three-dimensional structure of the shear layer in their numerical simulation. Research into the tone noise produced by jet–cavity interaction was carried out by Raman et al. [17]. They measured the emitted sound intensity and visualized the flow. Surprisingly, they pointed out that the tones for $L/D = 8$ corresponding to the acoustic modes of the cavity were independent of flow speed even

if the flow pattern showed a very complicated variation for flow Mach number. Rowley et al. [18] have carried out direct numerical simulation of two-dimensional compressible flow over rectangular cavities. They found a transition from a shear-layer mode for shorter cavities and lower Mach numbers, to a wake mode for longer cavities and higher Mach numbers. Also in their paper, the criteria for the onset of shear-layer oscillations and for the transition to wake mode are proposed. These criteria are based on linear theory for amplification rates in the shear layer, and a simple model for the acoustic efficiency of edge scattering.

As described above, the mechanism of self-sustained oscillation in the cavity is well explained as a feedback loop of acoustic and fluid dynamic instability in or over the cavity. As to the possible feedback mechanism, two are available, i.e. the acoustic feedback as a wave motion and the fluid dynamic feedback due to convective or viscous effects. Of course, the acoustic instability will induce the fluid dynamic instability in the shear layer. Hourigan et al. [19] have investigated the aerodynamic sources of acoustic resonance in a duct with baffles. They identified the source of sound in a cavity formed by baffles in a duct. As mentioned in that paper, it is very important to identify the sources of the feedback signal. More particularly for transonic flows, the acoustic and fluid dynamic effects interact with each other. As shown in Heller [7], the intensity of acoustic emission had a maximum in this region.

In the present paper, a sound resonance in a high-speed internal cavity flow was investigated experimentally. The measurement was carried out in subsonic region and free stream Mach number was varied from 0.5 to 0.85. The corresponding Reynolds number was varied from 3×10^5 to 4×10^5. When the flow Mach number approached unity, the resonance was excited due to the fluid dynamic resonance. In these flows, strong wave propagation was observed and the shear layer could oscillate strongly. In order to analyze the fluid dynamical resonance, development of the shear layer, streamwise and transverse disturbances, and vortex shedding should be studied in detail. In the present experiment, a high-speed video camera was used to capture the transient process from the start of flow to the periodic oscillation. After that, particle image velocimetry was used for the velocity measurement. Based on the experimental results, the velocity fluctuation and vorticity distribution in the cavity will be discussed.

2. Experimental technique

2.1. Experimental setup

A schematic view of the test section is shown in Fig. 1. The height, H, and the width, W, of the cross section are 20 and 25 mm, respectively. The depth of the cavity, D, is fixed at 20 mm and its length, L, is 20 mm or 40 mm. The corresponding length to depth ratios of the cavity, L/D, is 1 or 2. Fig. 2 shows the schematic of the experimental apparatus. An intermittent wind tunnel was used in the experiment. The test section was connected to a vacuum tank. Airflow started by rupturing the diaphragm. The duration time of steady flow was less than 2 s. A throat was located downstream of the test section to adjust the flow Mach number. The distance between the throat and the trailing edge of the cavity was 220 mm. The predicted temperature and velocity are shown in Fig. 3. These values

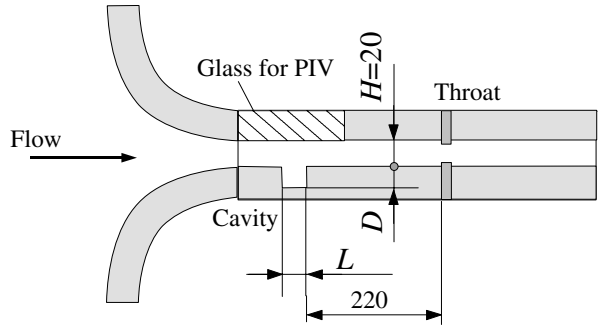

Fig. 1. Schematics of test section. $D = 20$ mm, $H = 20$ mm, $L/D = 1$ and 2.

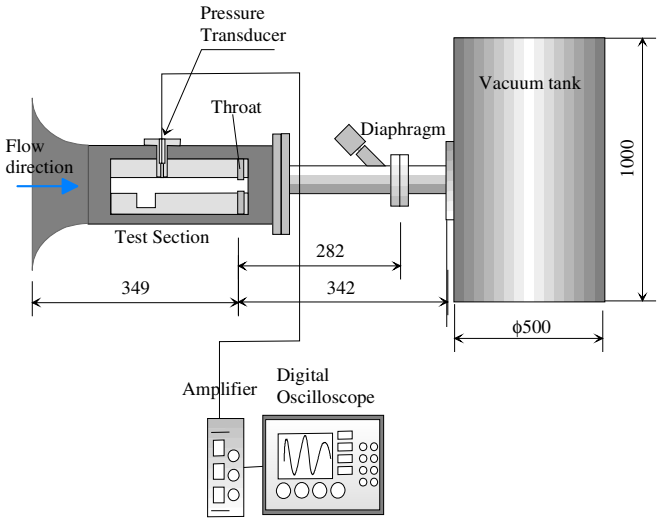

Fig. 2. Experimental apparatus.

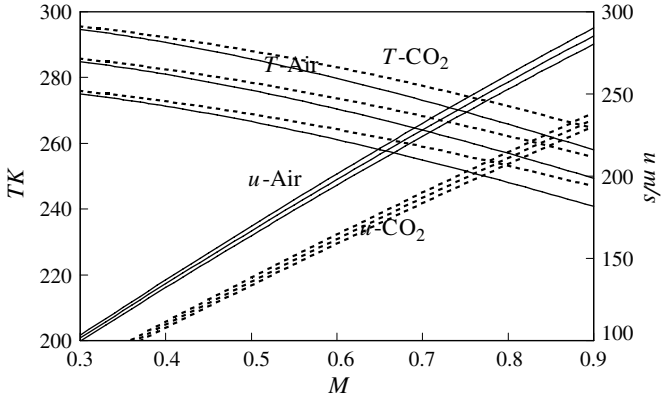

Fig. 3. Temperature and flow velocity versus Mach number in the present experiment.

were calculated with an isentropic condition. In the experiment, the stagnation temperature of the flow was about 290 ± 10 K. In the present study, we carried out experiments with atmospheric air, while in the PIV measurements, the working gas was CO_2. As described in Fig. 3, solid lines show T and u for the air, and a dashed line for CO_2. For air, the free stream velocity can be varied from 190 to 250 m/s by changing the height of the throat. Correspondingly, the flow Mach number was varied in the range from 0.5 to 0.85. The pressure in the flow was measured with a flush mounted transducer (Kulite XCQ-062-50A), which was located on the upper wall of the test section for the sound intensity measurement. The pressure signal was discretized and stored in a digital oscilloscope. The sampling rate and storage length of the pressure signal were 100 kHz and 160 kWords in 10 bits resolution, respectively. The spectral component of the digitized signal was analyzed with FFT on a personal computer. An isentropic process was assumed to determine the flow Mach number in free stream. The flow Mach number was calculated from the pressure ratio between the static pressure on the sidewall and the stagnation pressure using the standard one-dimensional adiabatic flow relationships.

The test procedure is described as follows. At first, the vacuum tank was evacuated to 10 Torr, then the diaphragm which separated the test section and the vacuum tank was ruptured by an air-driven spear. An expansion flow was thus induced in the test section. Through several preliminary tests, the time duration of the steady flow was ascertained to be for at least 1.5 s for all Mach number conditions. By triggering with the rapid drop of the pressure signal at the expansion, the flow visualization and pressure measurement were carried out.

2.2. Flow visualization

The schlieren system used in the present experiment is the same as described in Khan et. al. [20]. A high-speed CCD camera was used for the flow observation, which has been developed by Prof. Etho at Kinki University. The camera features include a high resolution in space, a high-speed frame rate and high sensitivity. The framing rate can be varied from 30 to 10^6 fps; moreover, the spatial resolution is kept as 312×260 pixels, which is the highest specification for high-speed video cameras in the same category of models. From these specifications, the frame interval can be varied from 33 ms to 1 μs. A halogen light of 300 W was used as a light source to capture the images. After preliminary experiments, it was found that the frame interval time of 16 μs was suitable for capturing the present unsteady flow process. Movies were acquired for both the starting process and the fully developed process. In the starting process, a shear layer was initially generated and gradually this shear layer interacted with the trailing edge of the cavity. The camera was activated by an external trigger signal from the pressure transducer when the diaphragm ruptured, then the images were captured from this instant. In order to observe the establishment of the fully developed flow, images were captured 5 ms after the diaphragm was ruptured. It was confirmed that self-excited oscillations had already started at that moment by observing the pressure signal. In Section 3, the flow pattern in the transient process will be analyzed, describing horizontal and vertical density fluctuations of the cavity for $L/D = 1$ and 2. Then, the fully developed flow in the resonant state will be discussed.

2.3. Particle image velocimetry

Fig. 4 shows the experimental setup for the particle image velocimetry (PIV) measurement. Aside from flow visualization, PIV measurement was carried out separately. A twin YAG laser was used for the illumination, with a light wavelength of 532 nm and a power of 50 mJ/pulse. The flow field was illuminated through the top window and the pressure history was measured on the sidewall of the cavity. PIV images were captured with the CCD camera, IDT-SharpVision ($1360\text{H} \times 1036\text{V}$ resolution, 10 bits in depth and minimum 200 ns in frame straddling separation). Images were acquired at the rate of 5 Hz. A pulse generator was used to synchronize the laser and CCD camera as the external triggering system. Data acquisition was carried out for the fully developed cavity flow. Phase locked data acquisition for the dominant frequency could not be achieved because the signal detection of resonant pressure was very difficult due to the low S/N ratio. Therefore, the present PIV data may show random data in the unsteady process. Water droplets, which were generated by a condensation technique with dry ice were seeded in the flow as a tracer. Therefore, the pre-mixed chamber was filled with CO_2 gas and water droplets. As shown in Fig. 3, since we used CO_2 as a test gas, the free stream velocity should be approximately 17% lower than for air. The nominal average diameter of the water droplets was 0.5 μm approximately. Water droplets were pre-mixed in a simple chamber which was connected to the test section.

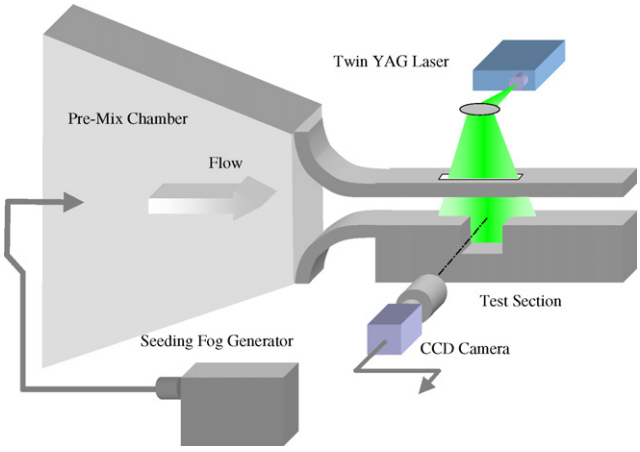

Fig. 4. Experimental apparatus for PIV measurement.

During the adiabatic expansion, whether the water droplets can exist or not depends on the state of the gas in the free stream and critical radius of the cluster. According to the preliminary test, the water droplets still exist in the free stream, so it was confirmed that this seeding method is acceptable for the present experiment. Time interval between the pair images was 500 ns. These pairs of images were analyzed with cross correlation calculation by using IDT-ProVision. The interrogation size used in the analysis was 32×32 or 64×64 pixels. For this inter-frame period, the displacement distance of seeded particles for the free stream velocity corresponded to about 5 pixels; the error vectors larger than 8 pixels were deleted from the data.

3. Experimental results and discussion

3.1. Strouhal number and pressure level

The frequency and the pressure level of the near field cavity tone were evaluated with the signal from the pressure transducer, which was mounted on the upper wall. A sound pressure level is defined in the conventional manner,

$$P = 20\log(\bar{p}_f/p_{ref}) \tag{3}$$

where, p_{ref} is the reference pressure, whose value is 20 μPa for sound in gases. $\bar{p}_f$ is the spectrum density of pressure amplitude. Here, we evaluated $\bar{p}_f$ as the square root of the power spectrum density, which was obtained from FFT analysis.

Fig. 5 shows two examples of the spectrum density of sound pressure for $L/D = 1$ and 2. Several discrete frequencies are observed in both figures (a) and (b). These frequencies correspond to the mode integers in Eq. (2). Through all the experimental data, the modes of the spectrum agree well with each other. However, the value of the spectrum density was scattered from one measurement to another. Consequently, the emitted sound intensity may be significantly sensitive to the initial flow condition, or its repeatability may depend on the instability of the feedback mechanism.

Fig. 6 shows the Strouhal number corresponding to the discrete frequencies, in which the data were picked up from the discrete frequency that appeared in the spectrum density distribution. The major four peaks were picked up from the spectrum density data and compared with Heller's prediction curves. As described previously, the combination of $\alpha = 0.25$ and $K_c = 0.57$ was used in Eq. (2). It is shown that the resonant frequency is well predicted by Eq. (2). In the low Mach number region, the experimental Strouhal number deviates from the predicted curves. Eq. (2) was derived for the fluid dynamic resonance, that is, the interaction between the vortices' convection and sound propagation, so that the deviation in the low Mach number region should be analyzed using fluid-resonant theory as pointed out by Rockwell [9].

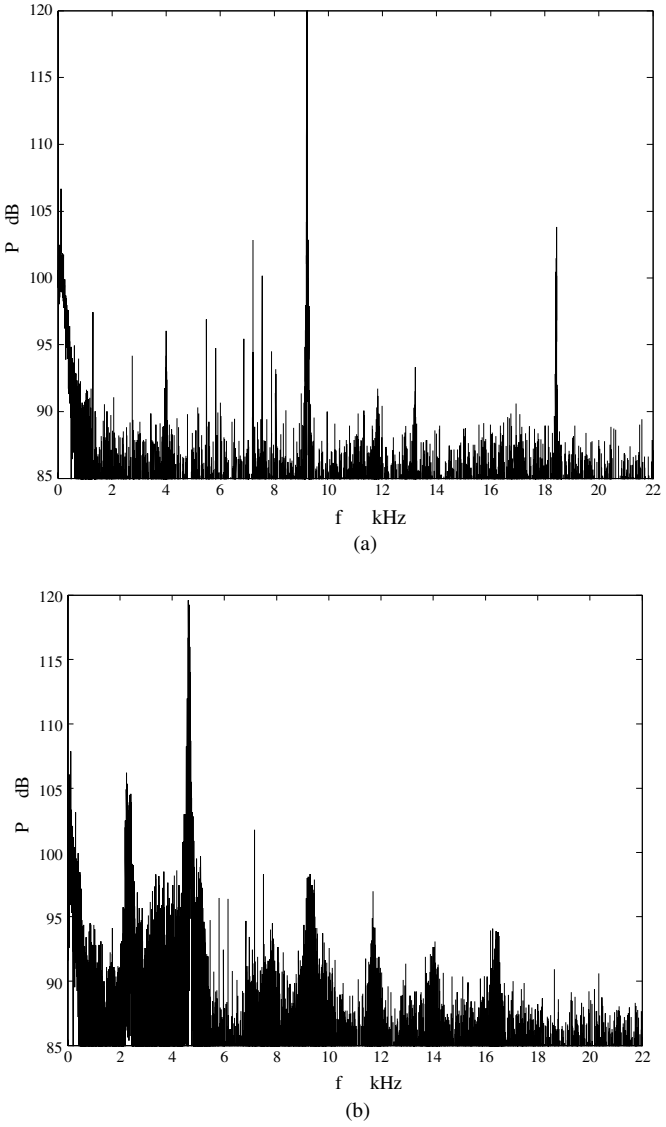

Fig. 5. Spectrum density of sound pressure level: (a) $L/D = 1$, $M = 0.74$, air; (b) $L/D = 2$, $M = 0.72$, air.

The prediction of sound pressure level is an important issue in addition to the frequency prediction. However, the pressure level is very sensitive to experimental conditions, such as upstream momentum thickness, turbulent intensity, surface condition around the sound source, etc. Fundamentally, it is very interesting to determine the Lighthill's stress tensor. However, the measurement is too difficult to compare the sound pressure by using the Lighthill [21], Curle's [22] equations with test data. In addition, in cavity problems, the fluid dynamic resonance is essentially nonlinear, so that a unique solution cannot be obtained analytically. In the present experiment, the sound pressure level was calculated from the pressure data with Eq. (3). The results are summarized in Fig. 7. Each data point in Fig. 7 was calculated for one experiment. In each experiment, the amplitude of the pressure was calculated with almost 100 kWords available data in 10 bit resolution. The data were acquired with 100 k samples per second.

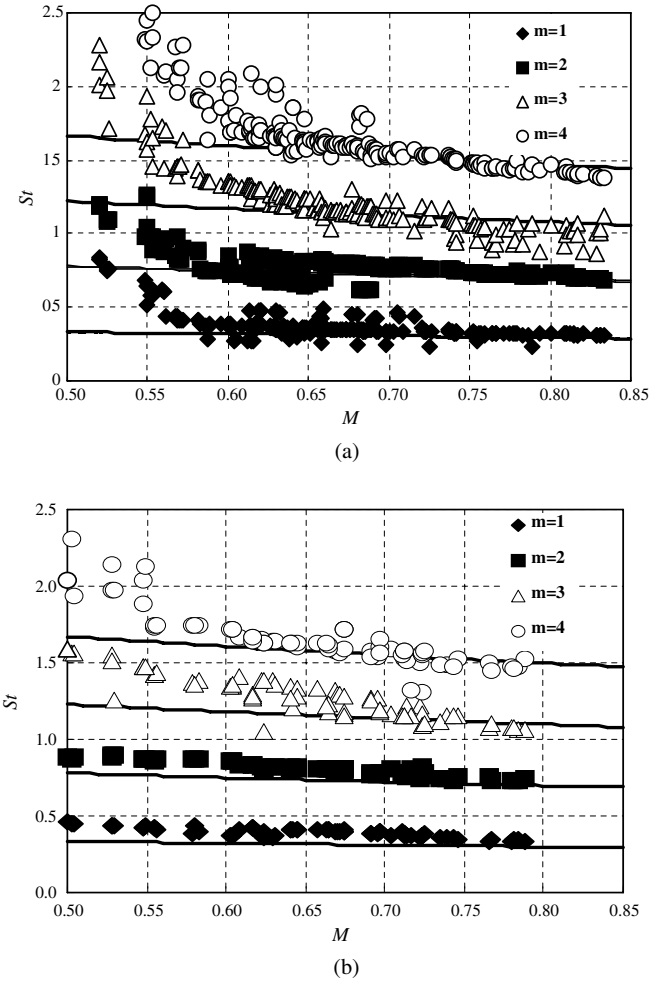

Fig. 6. Strouhal number. Solid lines show the Strouhal number by Eq. (2): (a) $L/D = 1$, air; (b) $L/D = 2$, air.

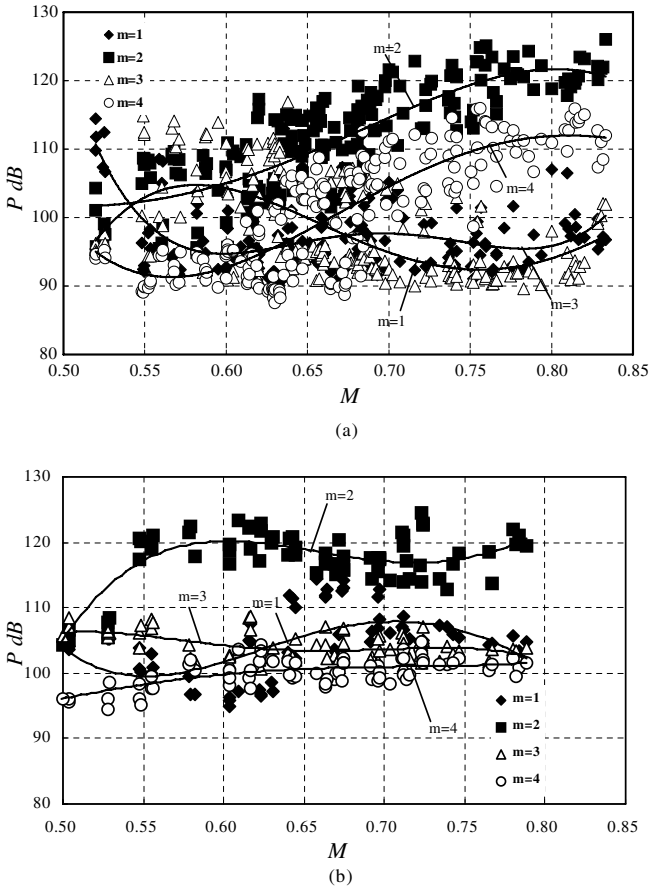

Fig. 7. Sound pressure level: : (a) $L/D = 1$, air; (b) $L/D = 2$, air.

Due to the limited time resolution, the experimental data are somewhat scattered. In Fig. 7, the biquadratic curves are fitted for each mode to indicate the variation of the mode vs. Mach number, however, the order of the fitting curves has no physical meaning. As shown in this figure, the sound pressure level becomes maximum at $m = 2$ for $L/D = 2$. On the other hand, for $L/D = 1$, P is large for $m = 1$ or $m = 3$ in the low Mach number region and $m = 2$ in $M > 0.64$. For $m = 2$, the flow mechanism was clearly confirmed with high-speed video camera, as discussed in the next section. It should be noted that the modal sound level increases with flow Mach number for $L/D = 1$ while it is almost constant for $L/D = 2$.

3.2. Pressure wave and vortices propagation

A conventional schlieren technique was applied for the flow observation. The knife-edge was placed at a horizontal setting (HS) to visualize the behavior of the shear layer, and a vertical setting (VS) to visualize the propagating wave and vortices. The typical schlieren photographs for $L/D = 1$ and $M = 0.79$ are shown in Figs. 8–10. Fig. 8 shows the starting flow. On inspecting the starting process, it is expected to observe the coherent structure of the undisturbed shear layer and the initiation of fluid dynamic instability. These pictures were captured immediately after the adiabatic expansion in the test section. Typical images showing the features of vortices' behavior were selected and are presented here. Tracking the vortices behavior, it is observed that a large vortex enters the cavity (Fig. 8(a)). The vortex collides with the trailing edge, and at the same time, the shear layer overreaches the cavity. That is, outgoing flow is observed near the trailing edge (Fig. 8(b)). In this manner, the shear layer is fluctuating due to the vortex entering and exiting the cavity. In Fig. 8(a) and (g) have almost same phase of the oscillation. Also, it should be noted that a very strong density gradient exists at the trailing edge when the vortex enters the cavity as shown in Fig. 8(a), (e), (f) and (g).

Fig. 9 shows the fully developed flow. The images are displayed with 32 μs intervals here, while images were acquired with 16 μs intervals in the experiment. Comparing Fig. 8 with Fig. 9, an apparent difference is recognized in the scale of vortices in shear layer. Relatively small vortices are observed in Fig. 8, while the vortices in Fig. 9 are relatively large due to the resonance. The shear layer in Fig. 9 is thicker than that in Fig. 8. Fig. 10 shows the VS obser-

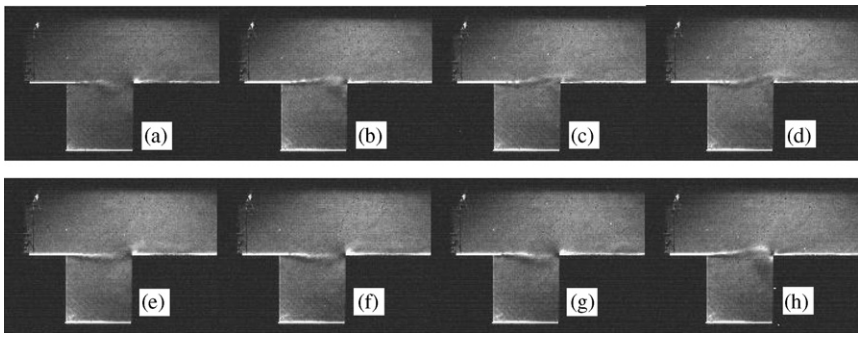

Fig. 8. Typical schlieren photographs of starting flow using high-speed video camera, HS, $L/D = 1$, $M = 0.79$, air, sequential left to right, delay = 0 s, +400 μs, +448 μs, +464 μs +528 μs, +560 μs, +592 μs, +688 μs.

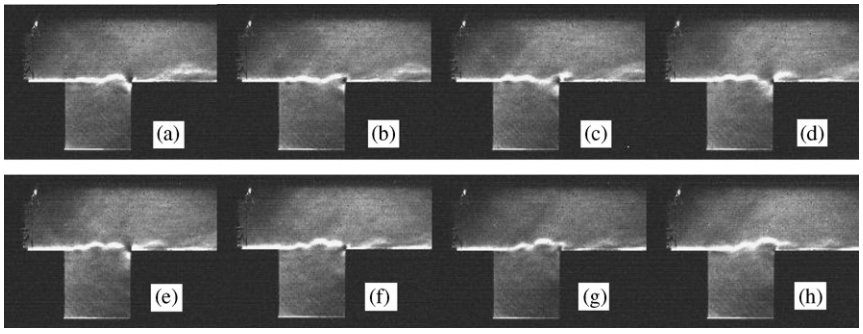

Fig. 9. Typical schlieren photographs of developed flow using high-speed video camera, HS, $L/D = 1$, $M = 0.79$, air, sequential left to right, delay = 5 ms, +32 μs increment.

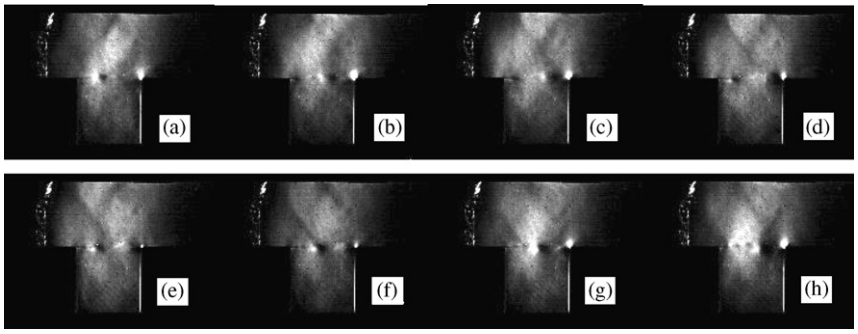

Fig. 10. Typical schlieren photographs of developed flow using high-speed video camera, VS, $L/D = 1$, $M = 0.77$, air, sequential left to right, delay = 5 ms, +32 μs increment.

vation of developed flow. In this observation, the horizontal fluctuation can be visualized clearly. The pairs of black and white spots in the shear layer correspond to a vortex and its boundary is the center of the vortex. We can identify the horizontal oscillation mechanism from these images. This behavior will be discussed and summarized in the following section.

Figs. 11–13 show the flow images for $L/D = 2$ corresponding to Figs. 8–10, respectively. In Fig. 11, the shear layer is rolling up in the cavity. Small vortices are observed in the shear layer; the scale of these vortices is independent of the feedback wave due to the large-scale coherent structure. The vortices move toward the trailing edge; the starting vortex becomes larger as the flow develops. At this stage, almost 20 small vortices have been generated in the rolling-up of the large-scale vortex in the cavity. Successive small vortices are observed at this instant. The time period for the generation of small vortices was about 1 ms. Of course, the scale and the shedding frequency of these vortices depend on the upstream flow conditions. The circulation in the cavity increases until the starting vortex occupies the whole region of the cavity. After this process, the starting vortex becomes unstable and flow separation was observed on the top of the trailing edge. The separation was induced by the outflow from the cavity. After several ms, a feedback sound wave reached the leading edge, which excited the development of a new vortex. This feedback process induced sound resonance in the cavity.

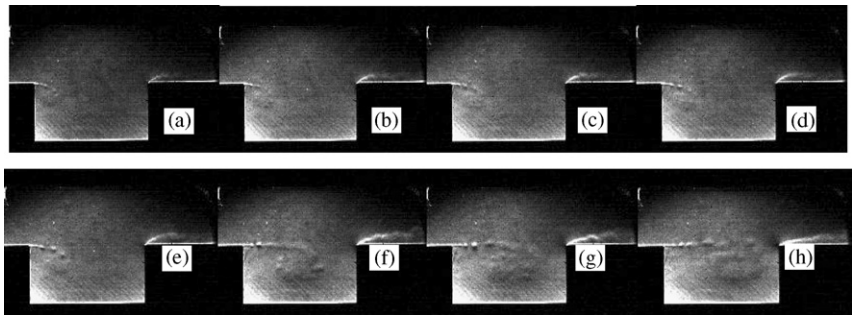

Fig. 11. Typical schlieren photographs of starting flow using high-speed video camera, HS, $L/D = 2$, $M = 0.77$, air, sequential left to right, delay = 0 s, +112 μs, +176 μs, +208 μs +304 μs, +848 μs, +944 μs, +1104 μs.

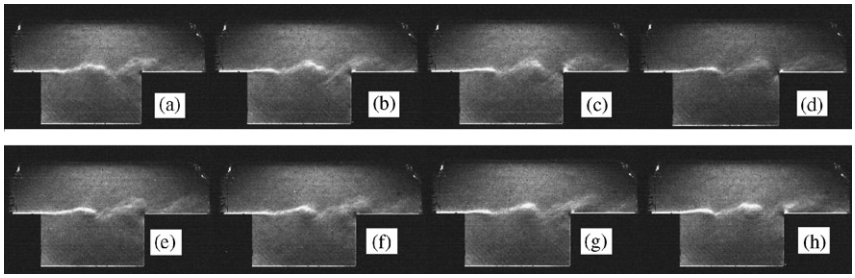

Fig. 12. Typical schlieren photographs of developed flow using high-speed video camera, HS, $L/D = 2$, $M = 0.76$, air, sequential left to right, delay = 5 ms, +32 μs increment.

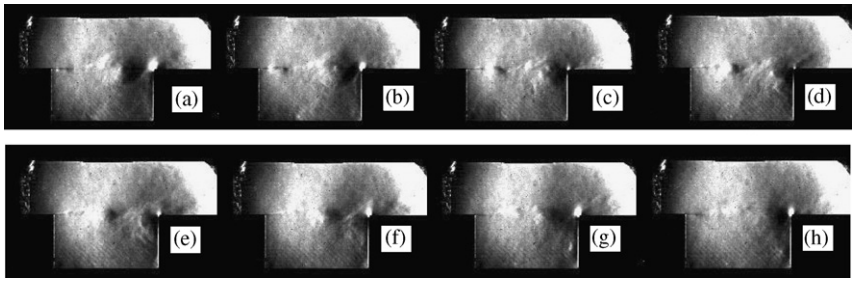

Fig. 13. Typical schlieren photographs of developed flow using high-speed video camera, VS, $L/D = 2$, $M = 0.75$, air, sequential left to right, delay =5 ms, +32 μs increment.

The periodic oscillations are shown in Figs. 12 and 13. In these video images, trains of two or three vortices are observed in the cavity. For $L/D = 2.0$, however, no apparent sound wave propagating upstream was observed in the experiment. If $x = 0$ at the leading edge of the cavity, the shear layer becomes very thick near $x = D$. It seems that the vortex undergoes a breakdown for $x \geqslant D$. The shear layer is disturbed downstream and interacts with the trailing edge.

In Fig. 14, the streamwise loci of vortices and compression wave are summarized in the $x - t$ diagram. Open and closed circles denote the pressure wave and the center of vortex, respectively. These loci were measured from the video images along the straight line crossing the leading edge and trailing edge of the cavity. The convection velocity of vortices is approximately 125 m/s. The wave propagates from right to left at 130 m/s in the laboratory coordinate. For the present experimental condition, the free stream velocity is about 250 m/s and the sound speed is 320 m/s. From these data, we obtain $K_c = 0.5$. This value is slightly smaller than the previously obtained value ($K_c = 0.57$). Furthermore, the estimated wave Mach number was 1.17. The Mach number was calculated as the ratio of the wave propagating speed and the sound speed in the free stream. Although the estimated Mach number is supersonic, it cannot be concluded immediately that the feedback wave propagates at supersonic speed. The temperature distribution in the cavity is not uniform but has a large gradient and the feedback wave in the cavity propagates faster than that in the free stream. When the compression wave reached the leading edge, the apparent vortical structure appeared in the shear layer. From the $x - t$ diagram, the compression wave encounters two vortices during its travel. Then, following Rossiter's model, it was confirmed that the mode integer m has a value of 2 in the present resonance. This fact corresponds to the

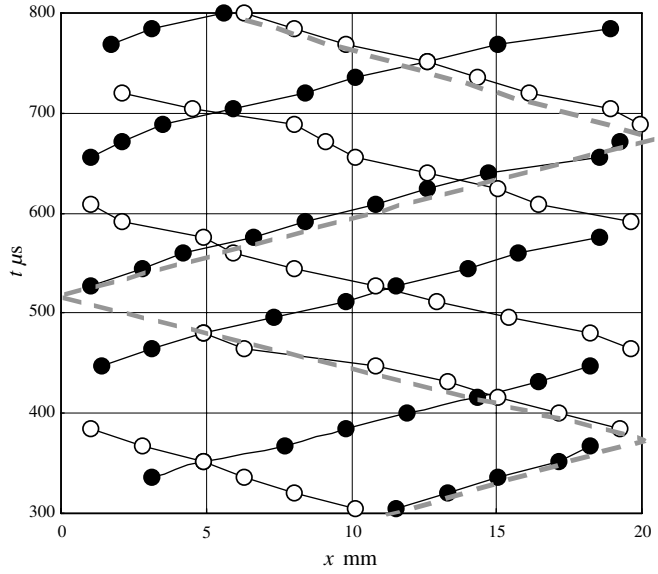

Fig. 14. $x - t$ diagram showing loci of vortices and propagating waves in the cavity, derived from high-speed video data, $L/D = 1$, $M = 0.77$.

observation that $m = 2$ is dominant in Fig. 7(a) for $M = 0.77$.

3.3. Instantaneous velocity distribution and fluctuation

Data acquisition of PIV images was carried out for the fully developed cavity flow, which was triggered by the pressure signal from the transducer on the side-wall. After rupturing the diaphragm, several pairs of images were stored in the PC. As stated in the previous section, it was difficult for the PIV data acquisition to be synchronized with the phase of the discrete noise due to the performance limitation of trigger devices. We started capturing images at 5 Hz using the pressure signal 5 ms after the adiabatic expansion. Steady flow continued for 1.5 s, which means that a maximum of 9 pairs of images could be obtained in one run. At least 6 pairs of images were obtained for the PIV measurement through all the experimental runs. Fig. 15(a) and (b) shows typical PIV images for $L/D = 1$ and 2, respectively. The tracer was introduced in the test section uniformly before the test started. However, it was difficult to keep a high number density in the cavity due to the entrainment and evaporation of water droplets after the flow start. Fig. 15(c) and (d) were taken to inspect the flow near the trailing edge in order to measure the vorticity near the corner. The inspection area size was 21.0 mm × 16.5 mm. As a preliminary measurement, the velocity of the free stream was measured and compared with the value estimated under the assumption of isentropic expansion. The difference between them was within 5%.

Figs. 16 and 17 show typical examples of visualization results. The instantaneous velocity vectors, streamlines and vorticity contours are presented for $L/D = 1$ and 2, respectively. As shown in Figs. 16(a) and 17(a), the velocity vectors were reconstructed well over the whole field. The free stream velocity is about 250 m/s at this condition, while the velocity is order of 10 m/s inside the cavity. It should be noted that, in spite of low tracer density in the cavity, a sufficient correlation was achieved from the images of the pairs in the cross correlation process. In Fig. 16, a large vortex appears in the cavity. Here, the vorticity was positive in the cavity. The shear layer was bent towards the cavity wall just before the collision on the trailing edge. On the other hand, in Fig. 17, two large vortices

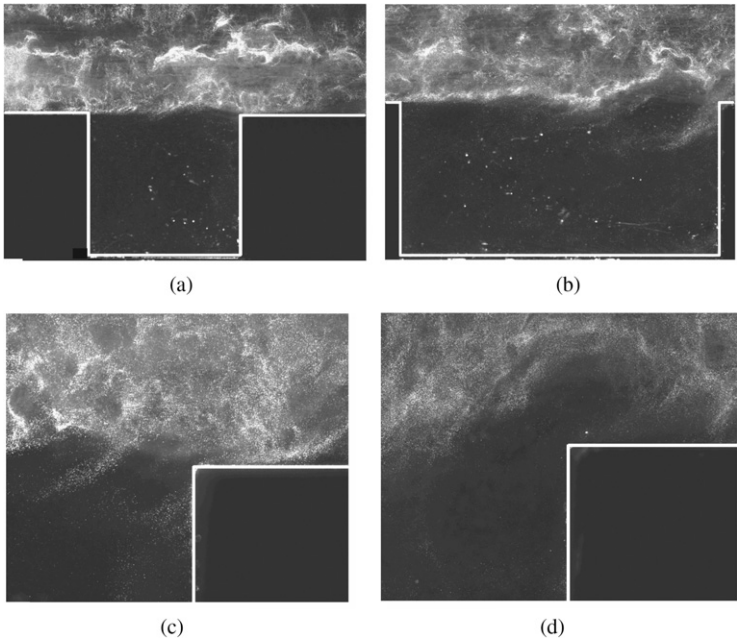

Fig. 15. Flow images obtained in PIV measurement: (a) $L/D = 1.0$, $M = 0.75$, whole field; (b) $L/D = 2.0$, $M = 0.65$, whole field; (c) $L/D = 1.0$, $M = 0.75$, near trailing edge; (d) $L/D = 2.0$, $M = 0.65$, near trailing edge.

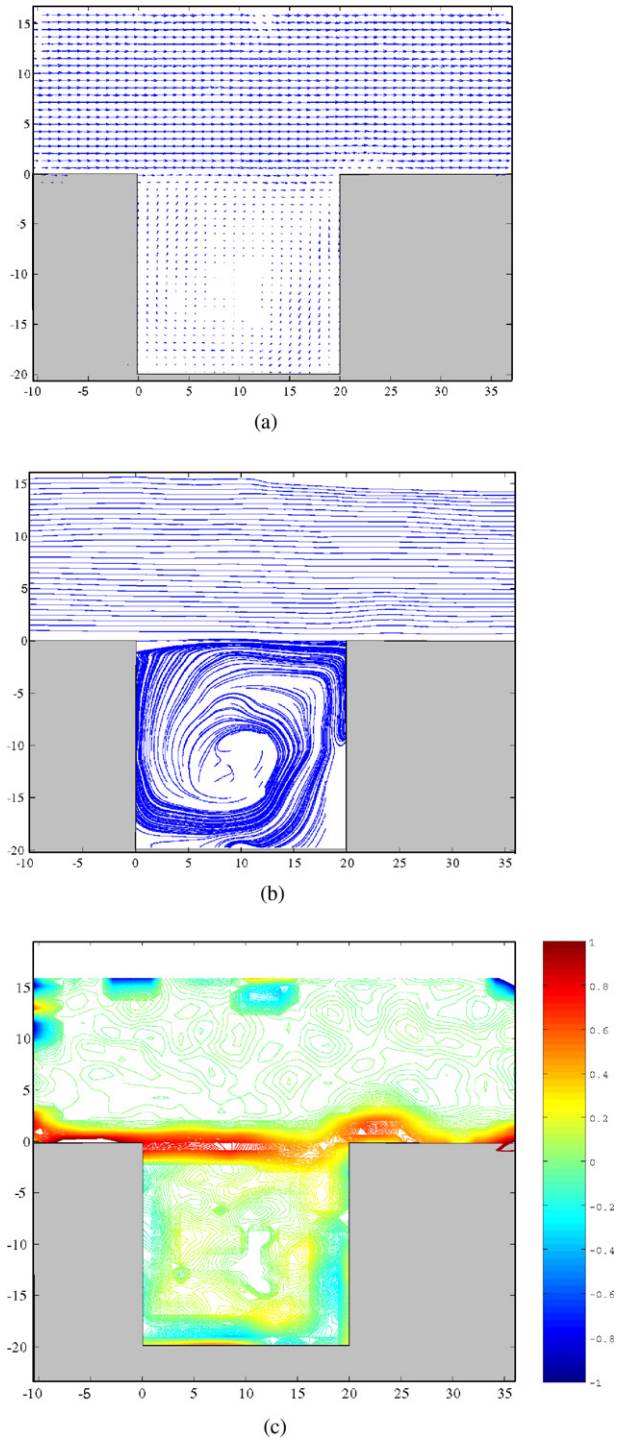

Fig. 16. Sample diagrams of instantaneous velocity vectors, streamlines and vorticity in the cavity flow of $L/D = 1$, $M = 0.75$, CO_2: (a) velocity vectors; (b) streamlines; (c) vorticity contours $\times 10^{-5}$.

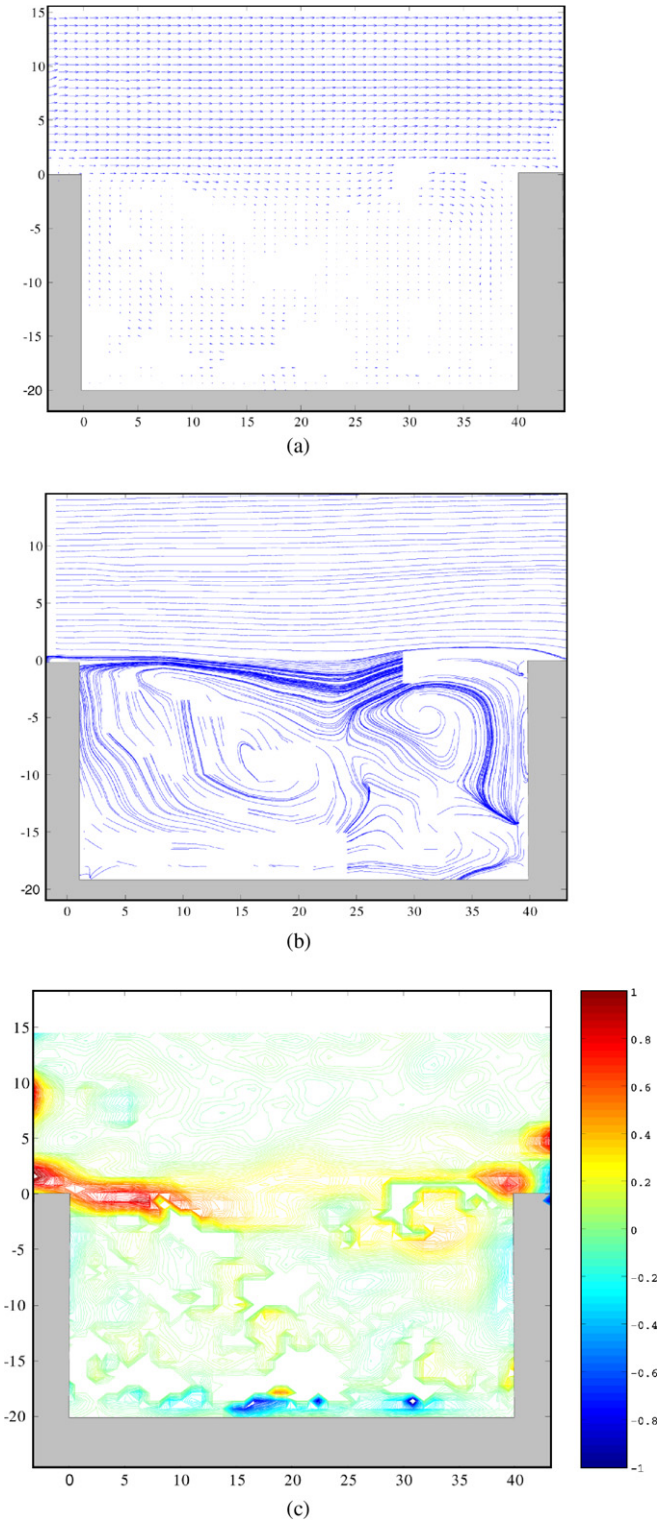

Fig. 17. Sample diagrams of instantaneous velocity vectors, streamlines and vorticity in the cavity flow of $L/D = 2$, $M = 0.65$, CO_2: (a) velocity vectors; (b) streamlines; (c) vorticity contours $\times 10^{-5}$.

are shown in the cavity. The streamlines shows a complex structure. The vortices in the shear layer curl around one another, and the width of the shear layer increases downstream. An incoming flow near the trailing edge is observed in the velocity vector and streamlines.

In order to observe the incident flow near the trailing edge, close up inspections were carried out. Figs. 18 and 19 show these results. Both of the figures show the instant of collision of a vortex with the trailing edge. Comparing these cases, the streamlines for $L/D = 2$ have a high magnitude of fluctuation than for $L/D = 1$. As shown in Fig. 19(b), the free stream fluctuates significantly due to

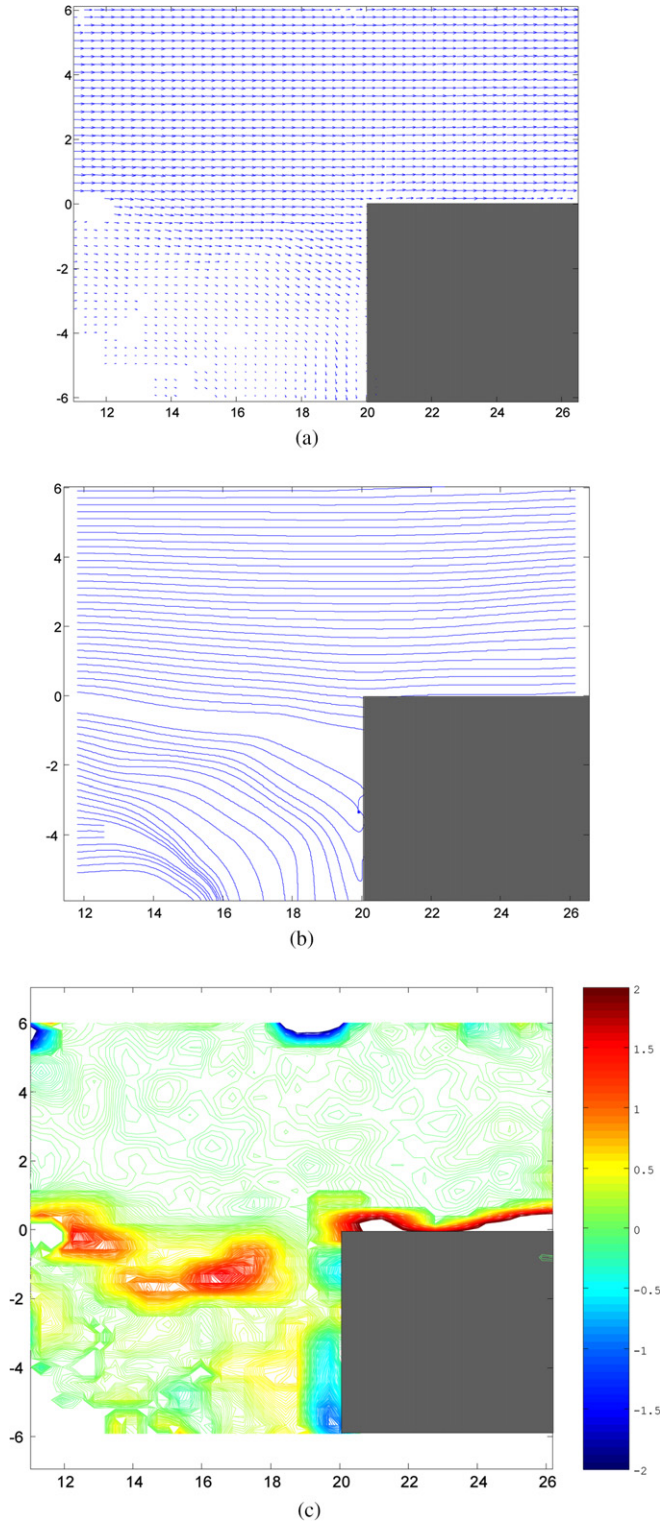

Fig. 18. Sample diagrams of instantaneous velocity vectors, streamlines and vorticity near the trailing edge of $L/D = 1$, $M = 0.75$, CO_2: (a) velocity vectors; (b) streamlines; (c) vorticity contours $\times 10^{-5}$.

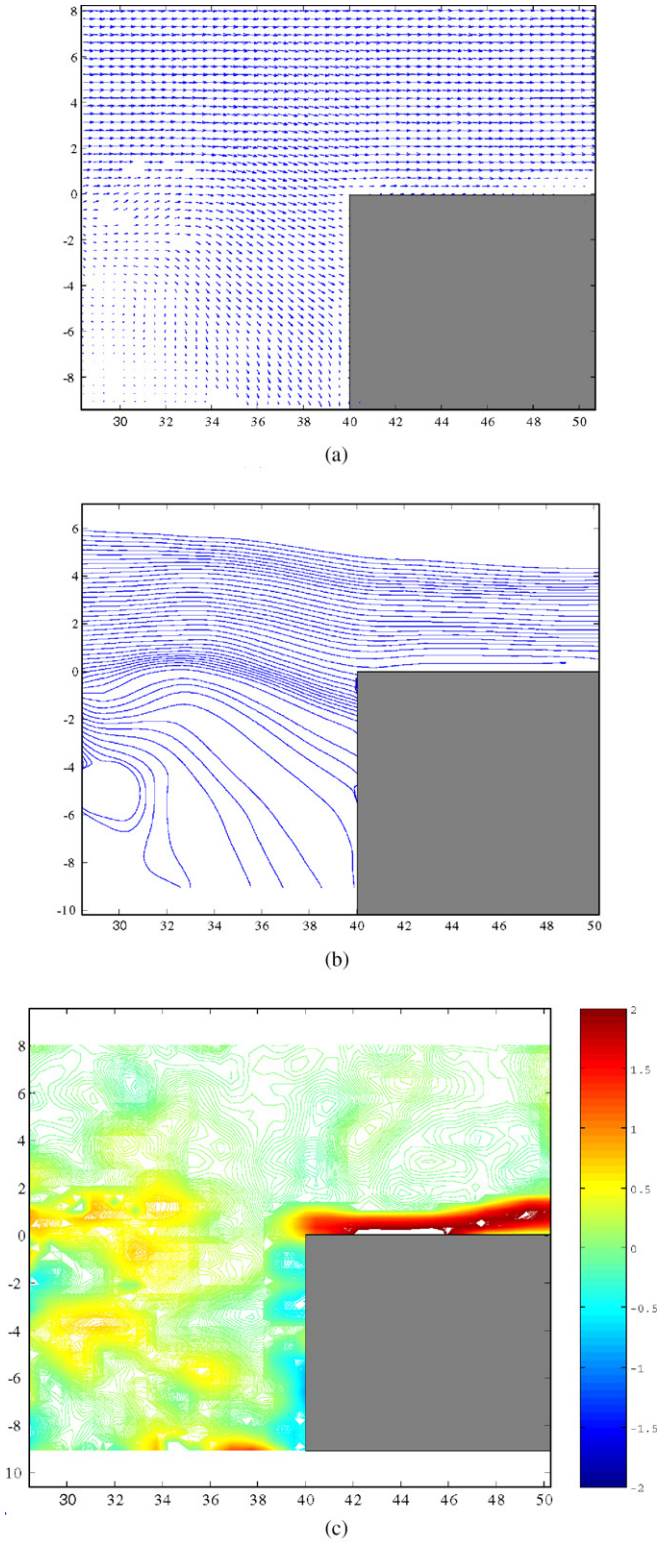

Fig. 19. Sample diagrams of instantaneous velocity vectors, streamlines and vorticity near the trailing edge of $L/D = 2$, $M = 0.65$, CO_2: (a) velocity vectors; (b) streamlines; (c) vorticity contours $\times 10^{-5}$.

the vortex oscillation. The shear layer instability develops downstream and a part of shear layer is defected downwards, whilst most of the flow passes over the trailing edge. The turbulence induces instability of free stream and its signal feeds back upstream. Whereas the investigation of the feedback mechanism is very important, in this section, we want to note the unsteadiness of the vorticity around the

trailing edge in order to consider the determination of the sound source. As shown in these figures, a strong fluctuation of vorticity was not evident at the front wall of the trailing edge. On the top wall of the trailing edge, a significant

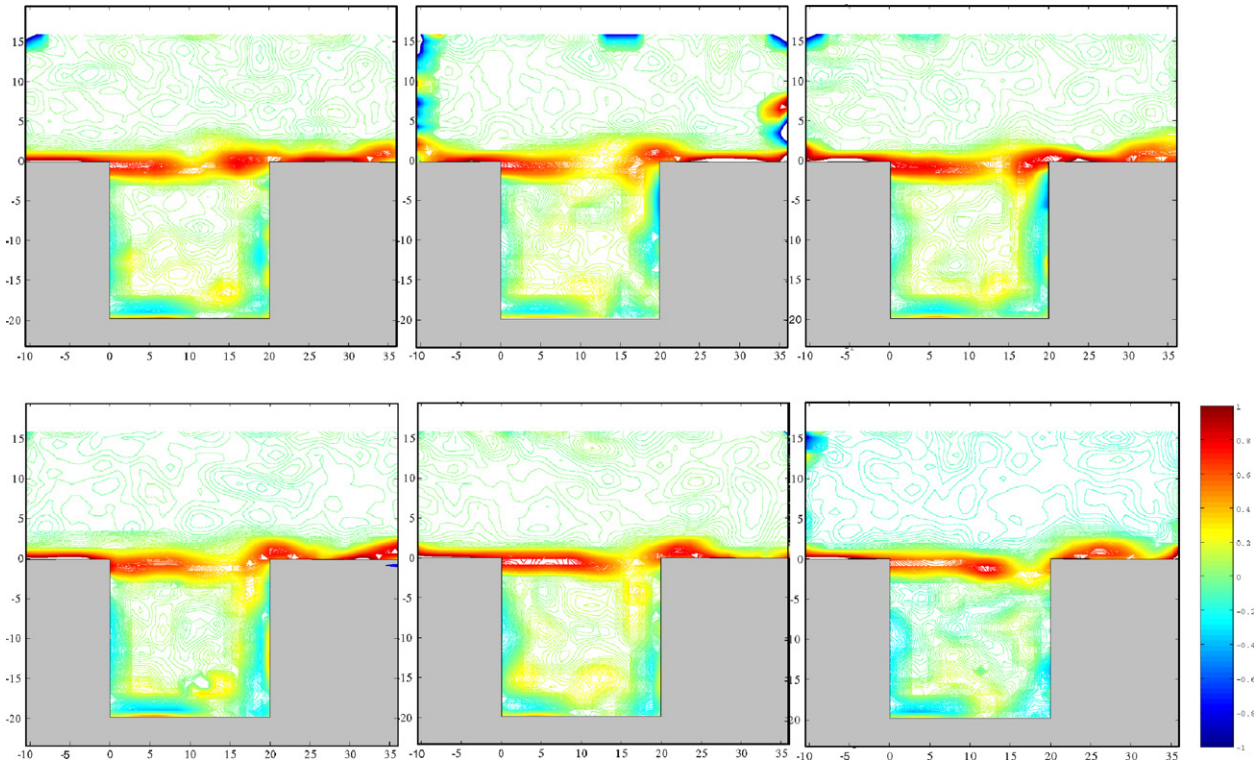

Fig. 20. Vorticity distribution $\times 10^{-5}$ in cavity flow for $L/D = 1$, $M = 0.75$, CO_2.

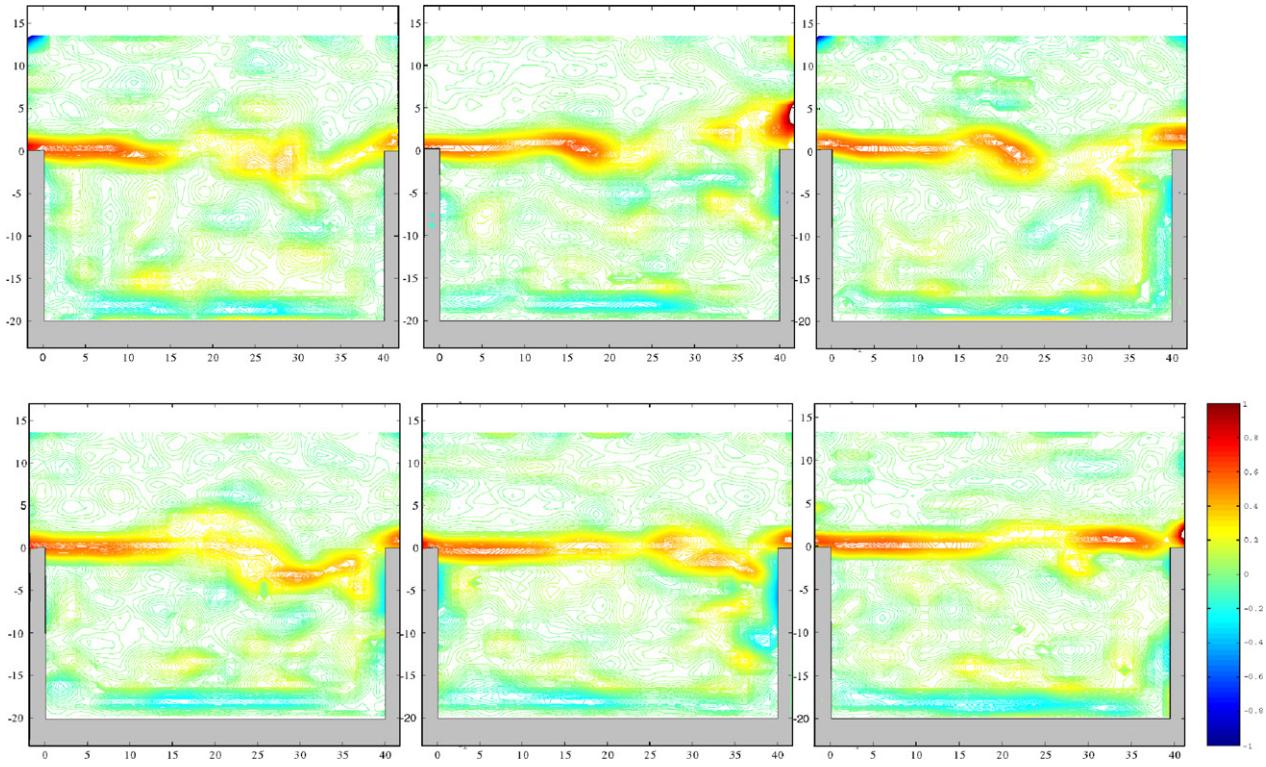

Fig. 21. Vorticity distribution $\times 10^{-5}$ in cavity flow for $L/D = 2$, $M = 0.65$, CO_2.

difference could be seen. Due to the instability of the shear layer, it was found that a very strong change of vorticity and detachment and attachment of boundary layer was induced at the trailing edge. However, it was not possible to determine the dipole behavior of the sound source in the present experiment. In order to determine the sound source as a dipole near the wall, one would have to carry out more precise experiments in the vicinity of the trailing edge.

Figs. 20 and 21 show the sets of vorticity distributions for $L/D = 1$ and 2, respectively. Although the Mach numbers are not same, the mode $m = 2$ is dominant in both cases (see Fig. 7(a) and (b)). These images were not obtained by the sequential data acquisition, but are rearranged in order based on the vortex pattern. In these figures, it is shown that the trains of vortices collide with the trailing edge, with part of each vortex then entering the cavity. For $L/D = 1$, after the vortex collides with the trailing edge, a small part of it flows into the cavity. For this flow condition, the resonant mode $m = 2$ exists as shown in Fig. 7(a). The main vortex in the cavity is oscillating. However, the amplitude seems to be small. Under such a condition, the harmonics should be developed due to the geometry of the cavity. The enhancement of the harmonics will depend on the flow linearity in the fluid dynamic resonance. Therefore, if the flow becomes nonlinear, the harmonics will be degenerated. For $L/D = 1$, the second harmonics for $m = 2$ is enhanced and is shown in Fig. 7(a). Under the condition, the vortical structure in the cavity does not show a significant fluctuation, so that the mode $m = 4$ has a relatively high acoustic level.

When $L/D = 2$ (Fig. 21), the vortex fluctuates significantly upstream of the trailing edge, and two or three vortical structure are observed in the cavity. Complex incoming and outgoing flows are formed near the trailing edge. The strength of vortices which collide with the trailing edge still has the same order as that in $L/D = 1$. The acoustic level is also of the same order as shown in Fig. 7(a) and (b). However, in this case, the vortical structure fluctuated significantly and the harmonics may not be well established. The second harmonics has relatively low level as clearly indicated in Fig. 7(b).

3.4. Mean flow profile

Mean velocity profiles for $L/D = 1$ are shown in Fig. 22. These mean profiles were calculated using 15 or 16 PIV data. However, the number of data points is not sufficient statistically; due to the limitation of the experimental devices, we could obtain only 3–6 data points for each experimental run. Therefore we conducted several runs to obtain the mean flow data. The profiles show the streamwise velocity distribution in the transverse sections at $x = 1/4L$, $1/2L$, and $3/4L$. The velocity profile corresponding to the shear layer is shown near $y = 0$. It can be seen that the thickness of the shear layer increases downstream. Since the free stream velocity is approximately 200 m/s and the shedding vortex velocity is half of the free stream

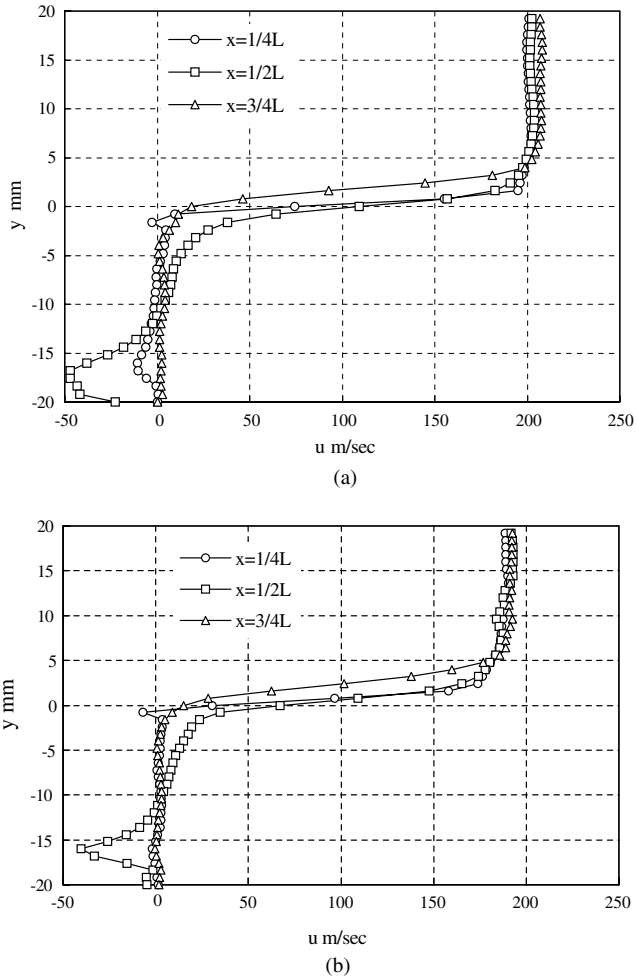

Fig. 22. Mean velocity profile for $L/D = 1$: (a) $M = 0.75$, CO_2; (b) $M = 0.65$, CO_2.

speed, the vortex convection velocity is estimated as about 100 m/s. In this profile, the middle point of the free stream velocity for $x = 3/4L$ lies above the other two lines. In addition, the free stream is accelerated slightly in the streamwise direction. In the cavity region, the velocity profile reveals a typical cavity flow pattern. In the region $y \leqslant -10$, namely the lower half region of the cavity, a negative velocity region is formed at $x = 1/2L$ and $1/4L$, but it is not evident for $x = 3/4L$. The shear layer is displaced outwards near to the trailing edge of the cavity.

Fig. 23 shows the velocity profile for $L/D = 2$. Comparing the profiles for $L/D = 1$ and 2, a significant difference exists between them qualitatively. A significant difference is evident at $x = 1/2L$. For $L/D = 2$, the obvious and stable vortical structure was not formed. The magnitude of the velocity in $0 \geqslant y \geqslant -10$ is positive and very small. This profile implies that a large and steady vortical structure did not form in the cavity. For $x = 1/4L$ and $3/4L$, we cannot see a symmetrical profile corresponding to the steady vortex. Therefore we can conclude that the shear layer was displaced outwards from the cavity and the flow is unstable outside of cavity.

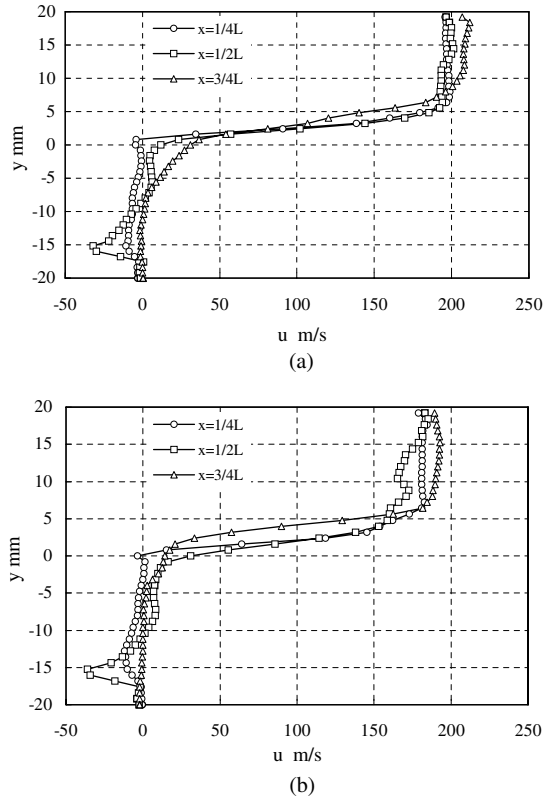

Fig. 23. Mean velocity profile for $L/D = 2$: (a) $M = 0.75$, CO_2; (b) $M = 0.65$, CO_2.

4. Concluding remarks

Fluid dynamical flow instability in cavity flows near transonic flow region was investigated experimentally. The acoustic pressure levels and velocity field were measured in cavities with a length to depth ratio of $L/D = 1$ and 2 at the free stream Mach number $M = 0.5$ to 0.85. The frequency and pressure levels of the near field cavity tone were evaluated and the Strouhal number was obtained as a function of flow Mach number. The variation with Mach number showed the same dependency as for previous experiments [5,6,9]. The pressure level of discrete frequency component and its harmonics were shown for a range of flow Mach numbers. The pressure level for mode number, $m = 2$, was the most intense for a wide range of flow Mach numbers. The relation between the modal sound pressure level and the flow Mach number shows a different distribution for $L/D = 1$ and 2. There was a remarkable difference in the sound pressure level of the harmonics for the two cases.

Flow observation and velocity measurements were carried out with a high-speed video camera and the PIV technique. The process from the initiation to the establishment of a resonance was observed with high-speed video visualization. By summarizing the loci of pressure wave and vortices in $x - t$ diagram, it was confirmed that the mode $m = 2$ is dominant in the present condition for $L/D = 1.0$. This process was compared with the result of velocity measurement using the PIV technique. In the PIV measurements, the evolution of the vortices in the cavity was shown quantitatively, highlighting the instantaneous vorticity just before the collision between a vortex and the trailing edge. The velocity distribution for a vortex that was shed from the cavity provides evidence of the fluid dynamic oscillation. A strong fluctuation of vorticity was observed around the trailing edge. In the present experiment, the results of the velocity measurement suggested the feasibility of determining the dynamics of sound generation near the trailing edge. However, in order to determine the sound source as a dipole near the wall, we would be required to carry out more precise experiments around the trailing edge.

References

[1] T.B. Owen, Techniques of pressure-fluctuation measurements employed in the RAE low-speed wind tunnels, AGRAD Report 172, 1958.
[2] D.A. Norton, Investigation of B47 Bomb Bay Buffet, Boeing Airplane Co. Document No. D12675, 1952.
[3] K. Krishnamurty, Acoustic radiation from two-dimensional rectangular cutouts in aerodynamic surfaces, NACA Technical Note, 1955, p. 3487.
[4] H.E. Plumblee, J.S. Gibson, L.W. Lassiter, A theoretical and experimental investigation of the acoustic response of cavities in an aerodynamic flow, WRDD-TR-61-75, 1962.
[5] J.E. Rossiter, Wind-tunnel experiment on the flow over rectangular cavities at subsonic and transonic speeds, Royal Aircraft Establishment ARC R&M, No. 3438, 1964.
[6] H.H. Heller, D.G. Holmes, E.E. Covert, Flow-induced pressure oscillations in shallow cavities, J. Sound Vib. 18 (4) (1971) 545–553.
[7] H.H. Heller, D.B. Bliss, The physical mechanism and flow-induced pressure fluctuations in cavities and concept for their suppression, AIAA Paper, 75-491, 1975.
[8] D. Rockwell, Prediction of oscillation frequencies for unstable flow past cavities, ASME J. Fluid Eng. 99 (1977) 294–300.
[9] D. Rockwell, E. Naudascher, Review of self-sustaining oscillations of flow past cavities, Trans. ASME, J. Fluids Eng. 100 (1978) 152–165.
[10] C.K.W. Tam, The acoustic mode of a two-dimensional rectangular cavity, J. Sound Vib. 49 (1976) 353–364.
[11] C.K.W. Tam, P.J.W. Block, On the tones and pressure oscillation induced by flow over rectangular cavities, J. Fluid Mech. 89 (2) (1978) 373–399.
[12] X. Zhang, J.A. Edwards, Computational analysis of unsteady supersonic cavity flows driven by thick shear layers, Aeronaut. J. 92 (919) (1988) 365–374.
[13] K. Sakamoto, K. Fujii, Y. Tamura, K. Matsunaga, Numerical analysis of a three-dimensional cavity flow field in a supersonic duct, JSME J. B 63 (606) (1997) (in Japanese).
[14] M.B. Tracy, E.B. Plentovich, J. Chu, Measurements of fluctuating pressure in a rectangular cavity in transonic flow at high Reynolds numbers, NASA TM-4363, 1992.
[15] Y. Takakura, F. Higashino, T. Yoshizawa, S. Ogawa, Numerical study on unsteady supersonic cavity flows, in: 27th AIAA Fluid Dynamics Conference, New Orleans, LA, 1996, AIAA 96-2092.
[16] Y. Takakura, F. Higashino, T. Yoshizawa, M. Yoshida, S. Ogawa, Parallel computations of unsteady supersonic cavity flows, in: A. Ecer, J. Periaux, N. Satofuka, S. Taylor (Eds.), Parallel Computational Fluid Dynamics (Implementations and Results Using Parallel Computers), 1995, pp. 59–66.

[17] G. Raman, E. Envia, T.J. Bencic, Tone noise and nearfield pressure produced by jet–cavity interaction, NASA-TM-20836, 1988.
[18] C.W. Rowley, T. Colonius, A.J. Basu, On self-sustained oscillations in two-dimensional compressible flow over rectangular cavities, J. Fluid Mech. 455 (Mar) (2002) 315–346.
[19] K. Hourigan, M.C. Welsh, M.C. Thompson, A.N. Stokes, Aerodynamic sources of acoustic resonance in a duct with baffles, J. Fluids Struct. 4 (345) (1990) 70.
[20] M.U. Khan, H. Hirahara, M. Kawahashi, Vortex shedding and wave propagation in transonic two-dimensional cavity flows, J. Visualization 3 (4) (2001) 331–339.
[21] S.J. Lighthill, On sound generated aerodynamically: I general theory, Proc. Roy. Soc. London A211 (1952) 564.
[22] N. Curle, The influence of solid boundaries upon aerodynamic sound, Proc. Roy. Soc. London A231 (1955) 505.